Journal of Remote Sensing
A SCIENCE PARTNER JOURNAL

RESEARCH ARTICLE

Distribution of Mangrove Species *Kandelia obovata* in China Using Time-series Sentinel-2 Imagery for Sustainable Mangrove Management

Chuanpeng Zhao[1,2], Mingming Jia[1,2*], Rong Zhang[1], Zongming Wang[1], Dehua Mao[1], Cairong Zhong[3], and Xianxian Guo[1]

[1]State Key Laboratory of Black Soils Conservation and Utilization, Northeast Institute of Geography and Agroecology, Chinese Academy of Sciences, Changchun 130102, China. [2]International Research Center of Big Data for Sustainable Development Goals, Beijing 100094, China. [3]Hainan Academy of Forestry (Hainan Academy of Mangrove), Haikou 571199, China.

*Address correspondence to: jiamingming@iga.ac.cn

Citation: Zhao C, Jia M, Zhang R, Wang Z, Mao D, Zhong C, Guo X. Distribution of Mangrove Species *Kandelia obovata* in China Using Time-series Sentinel-2 Imagery for Sustainable Mangrove Management. *J. Remote Sens.* 2024;4:Article 0143. https://doi.org/10.34133/remotesensing.0143

Submitted 29 September 2023
Accepted 27 March 2024
Published 15 April 2024

Mangrove management in China is converting from emphasis on occupied area to intrinsical quality. Mangrove species have varied ecological values, e.g., those having well-developed prop roots are more beneficial for coastal stabilization. The detailed distribution of mangrove species on a national scale remains a challenge, impeding species-specific applications in the ecology and management of mangroves, as well as evaluations of related Sustainable Development Goals. Although local-scale studies have explored various data sources, the variability of plant phenology is the key factor preventing their generalization from local areas to large latitudinal spans (e.g., the coast of China). The separability time period, defined by a separability metric for each scene of the image time series, provides a potential way to tackle the aforementioned problem. We conducted a case study on mapping *Kandelia obovata* in China based on Sentinel-2 time-series imagery, as it is a representative native mangrove species with the largest latitudinal span and tolerance to low temperatures. The proposed approach considered the separability between *K. obovata* and its typical co-occurring mangrove species, as well as that between *K. obovata* and salt marshes. The overall accuracy of the generated *K. obovata* map in China for 2020 reached 88.5% based on independently collected samples. The proposed approach is transferable to diverse mangrove species that inhabit a vast latitudinal span. The implications for sustainable mangrove management were discussed to reveal the benefits to precise management of mangroves, accurate biomass and carbon estimations accounting for species differences, and effective evaluation of mangrove ecosystem services.

Introduction

China is shifting from afforestation to ecological restoration with an emphasis on mangrove restoration in the Special Action Plan for Mangrove Protection and Restoration (2020–2025), which is issued by the Ministry of Natural Resources and the National Forestry and Grassland Administration. Mangrove restoration is tightly bound to mangrove species, e.g., *Kandelia obovata* has an impressive ability to withstand low temperatures, dominating mangrove poleward expansion to displace salt marshes under climate change [1,2]. With the largest latitudinal span in China, *K. obovata* has not been reported in the literature on its detailed distribution at the national scale, which impedes the implementation of precise management, accurate biomass and carbon estimations, and effective policies [3–5]. The habitats of this mangrove species have low accessibility due to the prevalence of tidal flooding, oxygen-deprived muddy substrates, and a profusion of thick trunks and aerial roots [6]. Therefore, remote sensing technology, which retrieves information through electromagnetic waves in a noncontact manner, provides the possibility of mapping nation-scale *K. obovata*.

Previous studies have focused on mangrove distribution, and some have attempted to identify and map local-scale mangrove species using various combinations of machine learning methods and diverse data sources [7–9]. These machine learning methods have varied forms, but their core is the same: determining decision boundaries in the designated feature space to minimize classification errors based on training data. As a field of machine learning, deep learning also follows the criteria, with the difference that they automatically derive features from larger amounts of labeled samples [10].

Unmanned aerial vehicles (UAV) carrying various payloads have provided multispectral, hyperspectral, and light detection and ranging (LiDAR) data at the centimeter level and guarantee fine discriminability between mangrove species [11]. However, UAV-based mangrove species mapping is limited to local areas on account of the expenses associated with data collection and the high processing pressure of acquired data [12].

High-resolution commercial satellites provide image scenes with a width of more than 10 km, importantly improving the efficiency of data acquisition, at the expense of a lower spatial resolution and limited payload. The acquired images typically have

4 multispectral bands and a meter-level spatial resolution, such as IKONOS, GF-2, and ZY-3. Studies have applied these commercial satellite images to map mangrove species and have confirmed that separability can be improved by using more spectral bands [13]. This was also proved by the emergence of applications that combined UAV-based payloads with such abovementioned multispectral images, even using the WorldView-2/3 with more than 8 spectral bands at a spatial resolution better than 0.5 m [14]. Consequently, applying these data to map mangrove species at a national scale still requires considerable cost and computational resources.

Medium-resolution satellites, which are freely accessible, have supported global-scale applications with the assistance of cloud computing platforms [15–17]. Regarding mangrove species mapping, efforts have been made to test the feasibility of using Sentinel-2, Landsat-8, and other data sources [18]. Sentinel-2 has been employed for mapping mangrove species distribution because of its multiple narrow red-edge bands and rapid revisit cycle [12]. At a local scale, plant phenology has been incorporated through harmonic analysis of Sentinel-2 image time series to improve mapping accuracy [19]. However, the variability in plant phenology along latitudinal gradients hampers the generalization of this approach to larger regional scales.

At the national scale, the median synthesis of Sentinel-2 image time series has been utilized for mapping the exotic mangrove species *Sonneratia apetala* in China [20]. The sensitivity of this mangrove species to chilling temperatures was used to determine the period for synthesis, and plant phenology was found to be dependent on latitude through case comparisons. This study obtained the first nation-scale distribution of a mangrove species; however, the approach may be difficult to generalize to other mangrove species, since native mangrove species have adapted to such temperature changes [21], especially to the mangrove species *K. obovata* which is tolerant to low temperatures.

An inspiration is that there may be a time period with higher separability because plant phenology is latitude-dependent [22,23]. The time period can be inferred through case areas in the southern and northern parts along latitudinal gradients using a separability metric with its typically adjacent mangrove species. Moreover, another time period representing the senescence season could enhance discrimination between *K. obovata* and salt marshes, as the former is evergreen and the latter withers in winter. In summary, dual-temporal imagery, composed of a high-separability time period and a senescence season time period, has the potential to achieve a national-scale *K. obovata* map.

To solve the problem of varied plant phenology and insensitivity to chilling temperatures in national-scale *K. obovata*, we proposed a new approach to map this mangrove species using dual-temporal Sentinel-2 imagery. This approach involves utilizing a high separability time period to distinguish it from typically adjacent mangrove species and a senescence season time period to differentiate it from salt marshes. The resulting *K. obovata* map of China can serve as a basis for monitoring mangrove expansion, estimating species-level biomass and carbon storage, and regulating management practices and policies.

Materials and Methods

Study area

The coastal regions in China where mangroves are distributed, along with their 1-km buffer zones, were determined as the study area, spanning from 18°09′N to 28°25′N (Fig. 1). The monsoon climate characterizes the area, with an obvious rainy season with high temperatures and a dry season with low temperatures. The dominance of the subtropical monsoon climate has facilitated the flourishing of cold-tolerant mangrove species, including *K. obovata*, due to winter air temperature extremes [24]. Moreover, human afforestation efforts have successfully transplanted *K. obovata* from its natural northern limit to the more northern Yueqing Bay, which was previously occupied by salt marshes [25,26].

The study object of this research is defined as a community vertically dominated by *K. obovata* in the upper canopy, in order to match the retrieved information from satellites. Although *K. obovata* is widespread, it is not always the dominant species in a region, as mangroves in China are characterized by widespread pioneer mangrove communities [27]. From the perspective of mangrove succession, *K. obovata* dominated mangroves are categorized as having a middle succession stage [28].

Data sources

Sentinel-2 imagery was acquired by 2 polar-orbiting satellites and exhibited a revisiting cycle of 5 d at the equator. Ten multispectral bands are usually applied, encompassing 3 visual bands (B2, B3, and B4), 4 narrow bands (B5, B6, B7, and B8A), 1 near-infrared band (B8), and 2 shortwave infrared bands (B11 and B12). Among the bands, the visual and near-infrared bands offer a 10-m resolution, and the remaining bands with a 20-m spatial resolution were resampled for consistency. Google Earth Engine facilitates processing because the surface reflectance product after preprocessing (e.g., topographic correction and atmospheric correction) can be easily accessed and processed to extract time-series information, and a cloud probability product was utilized to mask clouds and shadows.

To delineate the study area, a comprehensive map of China's mangroves in 2019 was chosen as an auxiliary data source (http://www.dx.https://doi.org/10.11922/sciencedb.00245). This map was derived from classification using Sentinel-1/2 and ALOS World 3D Digital Elevation Model (AW3D DEM) data and was carefully corrected using Google Earth images. After evaluation using 1,096 field sample plots implying mangrove survey expertise, an accuracy rate of 96.7% was achieved. Applying this mangrove map and its 1-km buffer zone as a constraint can improve the computational and correction efficiency.

Determining separability time period

Time period having higher separability with adjacent mangrove species

Plant phenology is ubiquitous for both deciduous plants in temperate regions and evergreen plants in tropical regions [29]. Mangrove species, which have undergone parallel evolution, belong to diverse families and genera [30], resulting in variations in plant phenology. Consequently, the separability between *K. obovata* and the other mangrove species can change over time. The key to this research was to determine a time period with higher separability from adjacent mangrove species.

Separability can be measured by the Jeffries–Matusita (JM) distance, which qualifies the separability between class pairs [31]. The JM distance falls within the range of 0 to 2, with a low value indicating that the 2 classes may be confused using the current feature set. In contrast to previous research that applied JM distance to evaluate feature combinations [32,33], we utilized

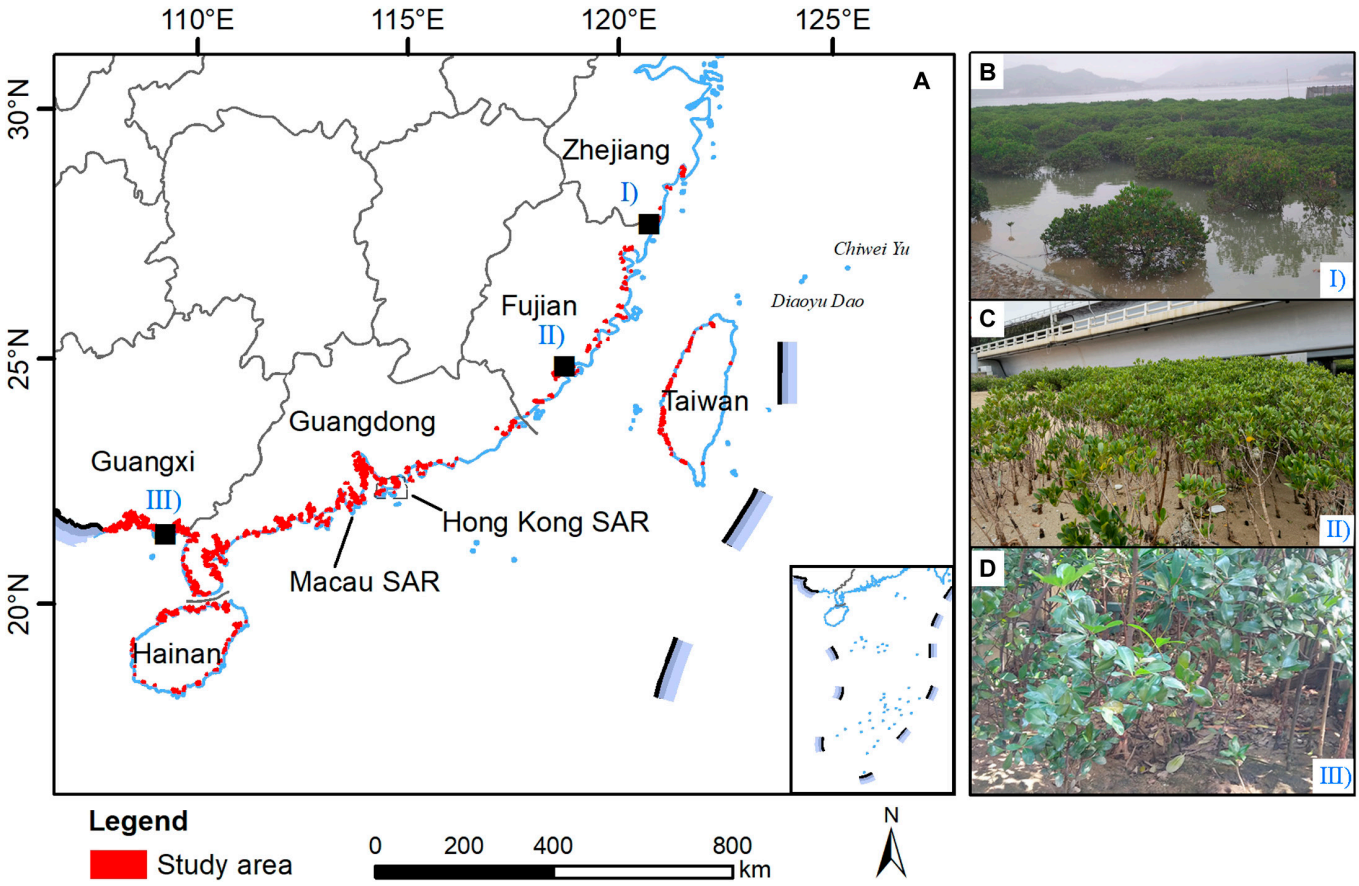

Fig. 1. Map of the study area (A). Pictures were taken during a field survey of (B) *K. obovata* at its natural northern limit and (C) an individual of *K. obovata*. The plots used the map with an approval number of GS(2024)0610 (D).

this metric to measure the separability between pairs of mangrove species using fixed samples and features.

Although latitudinal gradients along the narrow coast of China affect plant phenology, with varying temperatures, precipitation, and solar radiation, the time period can be inferred from at least 2 case areas. Considering the availability of mangrove species maps involving *K. obovata*, the northern case area was set as the Zhangjiang Mangrove National Nature Reserve in Fujian Province, and the southern case area was assigned as the Maipo Nature Reserve in Hong Kong. The northern case area was mapped using UAV-based optical and LiDAR data [34], as well as medium-resolution Sentinel-2 time-series imagery [19]. The southern case area integrated extremely detailed data sources, including multispectral imagery from a commercial satellite from WorldView-3 and UAV-based hyperspectral and LiDAR data [35]. The result using WorldView-2 imagery and a deep-learning-based method was also referred to [36]. The resulting mangrove species maps were georeferenced and vectorized to acquire the intended pairs of *K. obovata* and the common co-occurrence of *Avicennia marina* and *Aegiceras corniculatum*.

Using randomly selected sample polygons, the JM distances between *K. obovata* and *A. marina* and between *K. obovata* and *A. corniculatum* were calculated for each scene of Sentinel-2 imagery in 2020. The resulting JM distance time series showed different peaks and valleys in the northern and southern case areas. Considering the effects of clouds and shadows on optical imagery, we chose to perform a union operation to combine the peaks to augment the available Sentinel-2 imagery and finally determined the time period from 2020 April 13 to September 30. A median synthesis of these images during this time period was conducted to further reduce the impact of clouds and shadows.

Time period representing senescence season to eliminate salt marshes

The distribution of *K. obovata* partially overlapped with that of cold-tolerant salt marshes. Low-temperature stress drives this mangrove species to become dwarf shrubs, which are inconspicuous compared with flourishing salt marshes during the green-up season. *Spartina alterniflora* has invaded and rapidly expanded into dominant mangrove areas [37], which may also cause confusion between the 2 plant species in medium-resolution imagery. Moreover, native salt marsh vegetation, such as *Cyperus* spp. and *Phragmites* spp., can also occur near mangroves species [38]. To reduce interference from salt marshes, the time period between 2019 December 1 and 2020 March 1, when salt marshes were in dormancy, was chosen, and Sentinel-2 imagery acquired during this time period was synthesized using a median quantile for later classification.

Classifying based on machine learning

Classification features

Classification features define the feature space for inferring the decision surfaces. For each synthesized image representing the time period, we derived 45 classification features (Table 1),

including 10 image bands, 26 band ratios, and 9 typically used indices, as referenced in the literature [37,39,40].

We utilized the entire feature set for classification because feature selection methods tend to provide varied optimized feature sets, which is controversial for improving the classification accuracy. There is research advocating for improvement [41], while others argue that it does not typically enhance classification accuracy [42], and others contend that the effect of feature selection is related to the classification scheme as well as regional characteristics [43]. The impact of the feature selection is discussed in Impacts of different feature selection methods.

Classification samples

1. Designing the classification scheme

The distribution of the training samples served as the foundation for inferring a decision surface. In addition to the positive class *K. obovata*, the subclasses of the negative class should also be well-defined (Table 2). *A. marina* and *A. corniculatum* are mangrove species that typically co-occur with *K. obovata*; thus, they were emphasized by a large sample size. The emphasis was also applied to *Sonneratia* spp., which accounted for more than 11% of the mangrove area. *Bruguiera* spp. and *Rhizophora* spp. were assigned slightly smaller sample sizes. Mangrove species with small areas or limited distributions, including *Lumnitzera racemosa*, *Acrostichum aureum*, *Acanthus ilicifolius*, *Excoecaria agallocha*, and *Ceriops tagal*, were merged into the other mangrove subclasses. Outside the scope of mangrove species, nonmangrove vegetation near water [44], as well as salt marshes, were also taken into consideration due to potential confusion during classification; the subclasses of water, tidal flat, buildup, and cropland were merged into other nonmangrove subclasses.

2. Collecting and augmenting training samples

The training samples were collected in reference to the resulting pictures in the literature [34,45–50] with a supplement of field surveys and mangrove expertise. Field surveys were conducted between 2019 and 2023, encompassing areas such as Beihai in Guangxi Province, Gaoqiao in Guangdong Province, Fuding in Fujian Province, Hainan Province, and Shenzhen Bay. According to mangrove experts, *K. obovata* is the predominant mangrove species successfully introduced to a more northern

Table 1. Features derived from each synthesized image representing the time period having higher separability with adjacent mangrove species or salt marshes. Note: SWIR indicates B11 and B12, and RE in an expression refers to B5, B6, and B7. The involved expressions were calculated using each band to obtain different results.

Types	Expressions
Image bands	B2, B3, B4, B5, B6, B7, B8A, B8, B11, B12
Band ratios	B2/B4, B4/B2, B3/B4, B4/B3, B3/B8, B8/B3, B4/B5, B5/B4, B4/B8, B8/B4, B6/B5, B7/B4, B8/B2, B8/B5, B8/B11, B11/B8, B8/B12, B12/B8, B5/B3, B6/B3, B7/B3, B8A/B3, B8A/B5, B11/B12, B12/B4, B12/B11
Index features	$NDVI = \frac{B8-B4}{B8+B4}$ $NIRv = B8 * \left(\frac{B8-B4}{B8+B4}\right)$ $NDRE = \frac{B8-RE}{B8+RE}$ $LSWI = \frac{B8-SWIR}{B8+SWIR}$ $EVI = \frac{B8-B4}{B8+6*B4-7.5*B2+1}$ $PSRI = \frac{B4-B2}{B6}$

Table 2. The classification scheme in this research

Class	Subclass	Sample size	Description
Positive class	*Kandelia obovata*	1,000	Woody vegetation in the form of trees and sometimes in shrubs in an unsuitable climate
Negative class	*Avicennia marina*	150	Typically co-occurred with the target
	Aegiceras corniculatum	150	Typically co-occurred with the target
	Sonneratia spp.	150	Widespread in mangroves
	Bruguiera spp.	75	Sometimes co-occurred with the target
	Rhizophora spp.	75	Sometimes co-occurred with the target
	Other mangroves	100	Including *Lumnitzera racemosa*, *Acrostichum aureum*, *Acanthus ilicifolius*, *Excoecaria agallocha*, and *Ceriops tagal*
	Nonmangrove vegetation near water	100	Referring woody vegetation in the edge of near water bodies and tend to be misclassified as mangroves
	Salt marsh	100	Halophytic vegetation in the form of herbs, grasses, and low shrubs
	Other nonmangroves	100	Including water, tidal flat, buildup, and cropland

area than its natural northern limit. Regarding the time lag between the literature and the study period, we utilized visual checks and corrections based on Google Earth pictures to remove the changed or misclassified sample points.

The priori designed classification scheme and the collected training samples were put into the classification method to retrieve an initial classification result, which may have contained substantial cognitive biases because this research was the first attempt to map *K. obovata*. We interpreted the classification results and collected false-positive pixels to further augment the training samples. The procedure was iterated until the classification result converged, with the help of visual judgement. The final training samples consisted of 2,600 positive samples and 5,200 negative samples, which is consistent with the small proportion of *K. obovata*.

The priori designed classification scheme and training sample composition provided details of the starting position for the iteration and assisted in the reproduction of the research results. For the training sample composition after the iteration, an interpretation requires precise mangrove species distribution maps that are not currently available. This is beyond the scope of this study.

Classification method

The random forest (RF) algorithm was used to identify *K. obovata* using the provided features and training samples because of its wide application and high computational efficiency in land cover classification [51]. The Google Earth Engine served as the platform for executing the RF classifier with the hosted Sentinel-2 time-series images as the input. Adhering to Belgiu and Drăguț [51], the number of decision trees was constrained to 500, whereas the number of input features randomly selected at each node was determined to be 7 using the *randomForest* package in the local R environment.

Deep learning methods were not selected because of the scarcity of training patches at the national scale. Compared with sample points, training patches require detailed boundaries to separate *K. obovata* from other land cover types, which is more challenging than determining the presence of *K. obovata* at a location point. The results of this research can provide boundaries to support the development of deep-learning-based identification of *K. obovata*.

Postprocessing the classification result of *K. obovata*

The classification result requires further correction through postprocessing, which is a typical procedure in studies mapping mangrove distribution [44]. Moreover, postprocessing is required because of the challenge in mapping mangrove species, as these mangrove species share similar environmental characteristics [7,52].

The postprocessing consisted of 3 steps. First, northern mangroves located nearby or beyond the natural northern limit were assigned as *K. obovata* to reduce omission errors, as these patches are always in small areas due to climate constraints and can hardly be identified through classification alone [53]. Second, the remaining patches were processed with reference to the adjacent large-area patches when they had lower uncertainty. Finally, the postprocessed results were reviewed in cooperation with mangrove experts to refine the mapping results further. The abovementioned postprocessing served as a guarantee for the validity of the produced map.

The workflow for mapping *K. obovata* based on dual-temporal Sentinel-2 imagery is shown in Fig. 2.

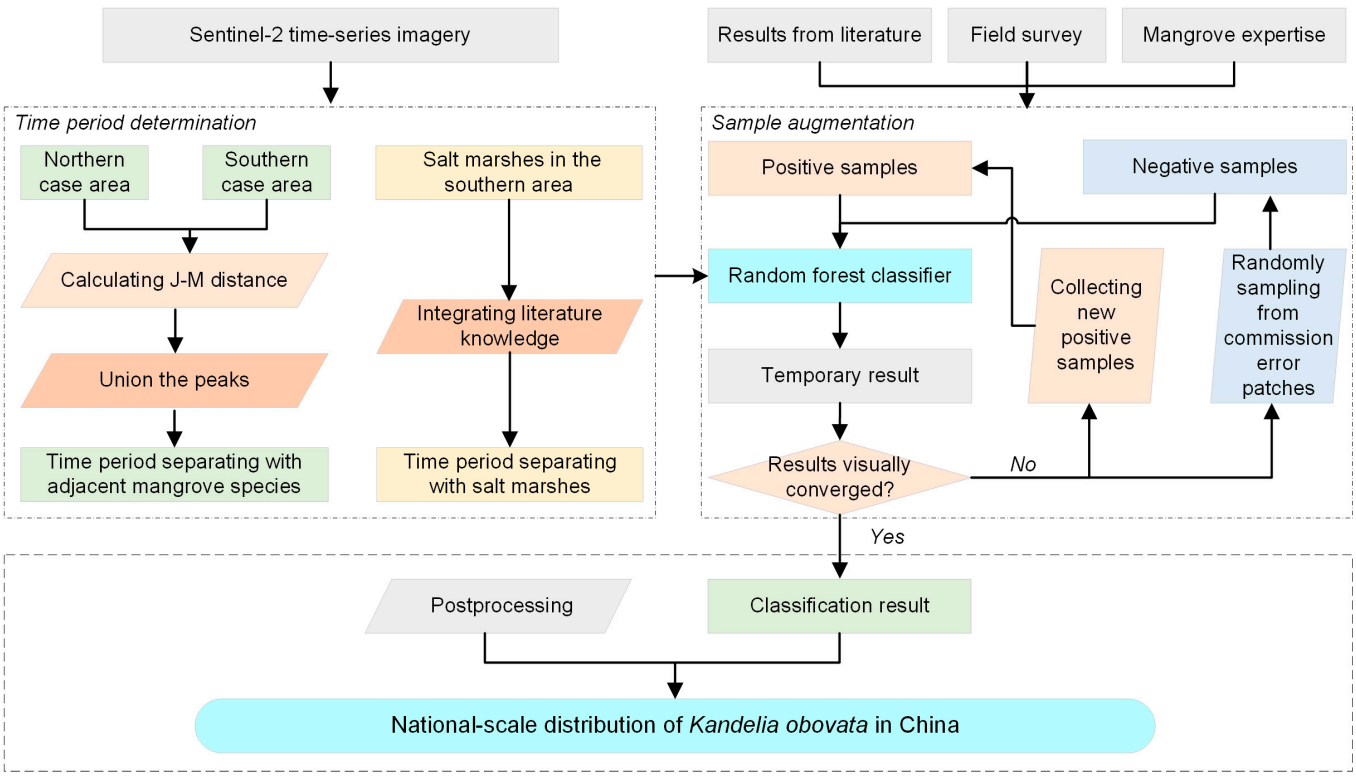

Fig. 2. Workflow for mapping *K. obovata* based on dual-temporal Sentinel-2 imagery.

Evaluations

The generated *K. obovata* map was evaluated using a validation dataset. We collected 759 positive samples and an equal number of negative samples through independent random sampling (Fig. 3A; sampling was not limited to the study area to ensure a more comprehensive evaluation). These sample points were not used for classification. Based on the constructed confusion matrix, the overall accuracy (OA) was employed to evaluate the accuracy of the generated map, and the metrics of the producer's accuracy and user's accuracy were also analyzed.

Qualitative comparisons were also performed using these 2 case areas (Fig. 3B and C). In addition to the 2 studies used for calculating separability between *K. obovata* and its common co-occurring mangrove species [19,35], we also acquired results using UAV-based optical and LiDAR data and the maximum likelihood classification method in the Zhangjiang Mangrove National Nature Reserve [34], as well as results obtained using commercial satellite imagery from WorldView-2 and a deep learning method [36]. These comparisons provide further detailed information on the generated map.

Results

The generated map shows that *K. obovata* was widespread in the study area (Fig. 4). The statistics showed that the total area of *K. obovata* in China for 2020 was 1,199 ha, among which Fujian Province has the largest area of mangrove species, followed by Hong Kong and Guangdong provinces. This also indicates that, although *K. obovata* can occur in various regions, only a few of them become dominant species occupying the upper canopy.

Based on the independently collected evaluation sample points, the generated national-scale *K. obovata* map achieved an OA value of 88.5% (Table 3). Specific to the mangrove species, the accuracy of patches annotated as *K. obovata* in the thematic map was 98.2%. However, the misclassification of *K. obovata* as another land cover type is key to further improve the OA value in future research.

Qualitative comparisons showed that the maps were generally consistent, although some differences were still present (Fig. 5). In the northern case area, the local map based on UAV captured more patches than the one using Sentinel-2 time-series imagery, while the generated national-scale map may have misclassified some other mangrove species as *K. obovata*. In the southern area, Li et al. [35] provided a mixed class of *K. obovata* and *A. ilicifolius* in addition to the target mangrove species. Considering that *A. ilicifolius* is a spiny semiwoody evergreen shrub that lacks a height advantage [54], observations from satellites may primarily capture the dominant canopy signals of *K. obovata*. Consequently, the local map based on similar high-spatial-resolution imagery incorporated the mixed class into *K. obovata*. The generated national-scale map achieved consistent results in the case area, which had large patches of *K. obovata*.

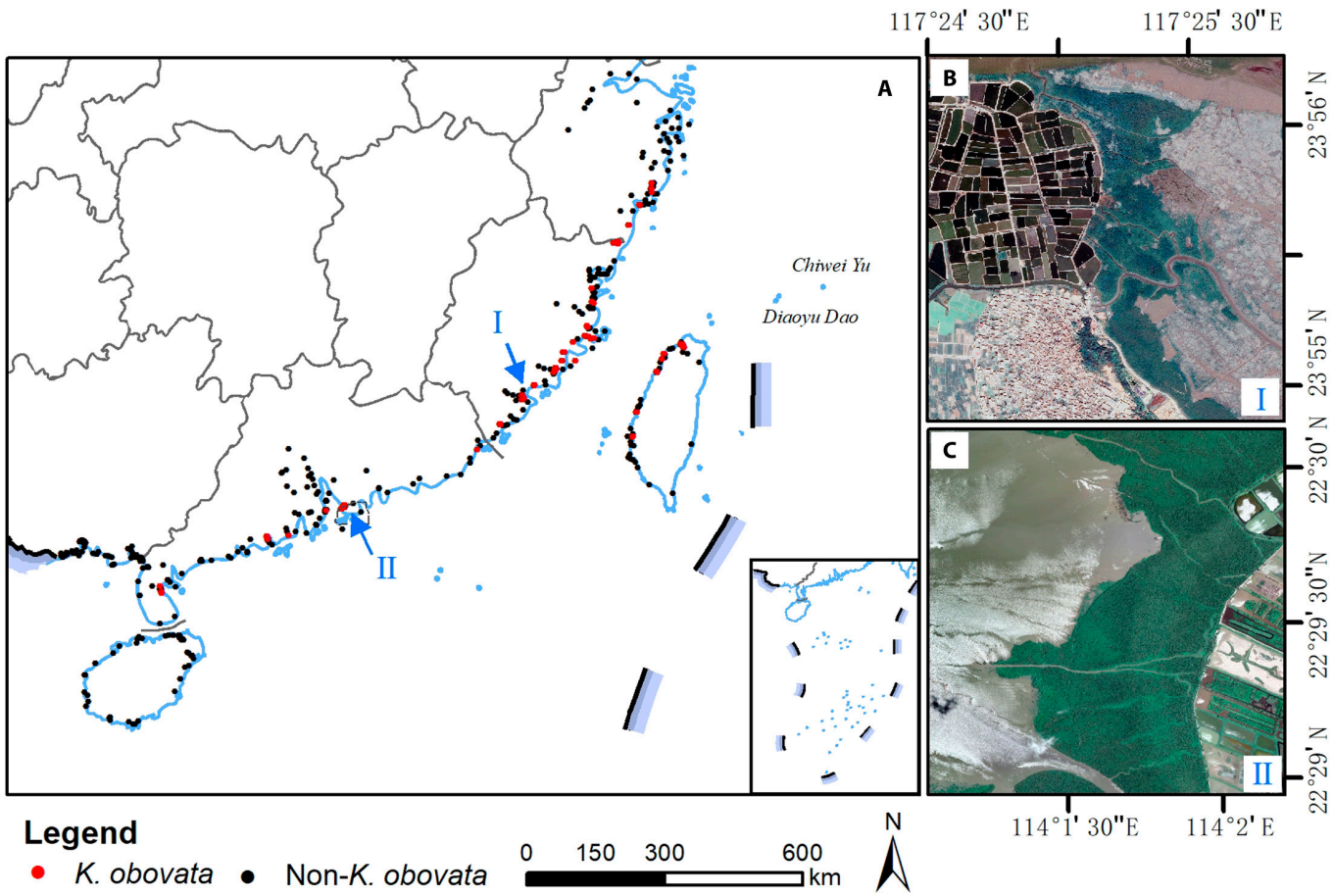

Fig. 3. Distribution of independently collected sample points for evaluating the generate map (A). Qualitative comparisons were executed using (B) the northern case area and (C) the southern case area, with the background using true-color Google Earth images. The plots used the map with an approval number of GS(2024)0610.

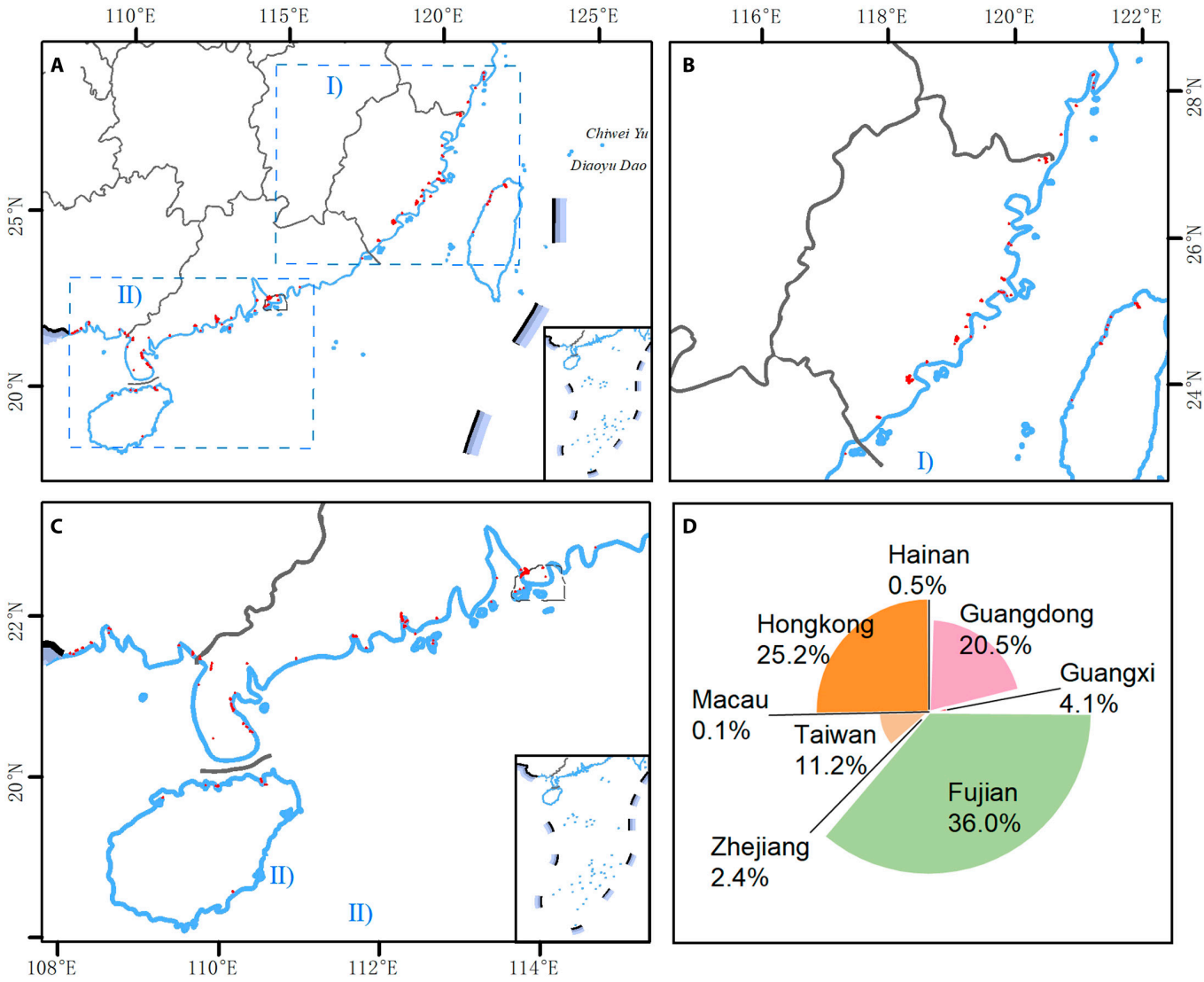

Fig. 4. The generated map of *K. obovata* in China for 2020. The details of its spatial distribution are shown in (A) to (C), and the area proportions for each provincial administrative region are in (D). The plots used the map with an approval number of GS(2024)0610.

In summary, both quantitative and qualitative evaluations indicate that the generated map provides details on the national-scale distribution of *K. obovata*. Therefore, the research achieved the objective to make the first attempt on mapping this mangrove species at a national scale.

Discussion

Advantages of the approach

Mangroves are evergreen communities that thrive in harsh environments characterized by tidal inundation and muddy anaerobic soils, leading to low intraclass separability. The latitudinal gradients along the coast of China result in changes in phenology [22], causing high interclass variability. Combined with the fact that harsh environments limit the acquisition of sufficient samples, classification of mangrove species is challenging.

In local areas, the application of UAVs to map mangrove species is gaining attention from researchers [11,34], as they can collect high-quality sample points by controlling the purity

Table 3. Confusion matrix of the generated *K. obovata* map in China for 2020

	Reference		
	Kandelia obovata	Non-*Kandelia obovata*	User's accuracy
Kandelia obovata	595	11	98.2%
Non-*Kandelia obovata*	164	748	82.0%
Producer's accuracy	78.4%	98.6%	
Overall accuracy			88.5%

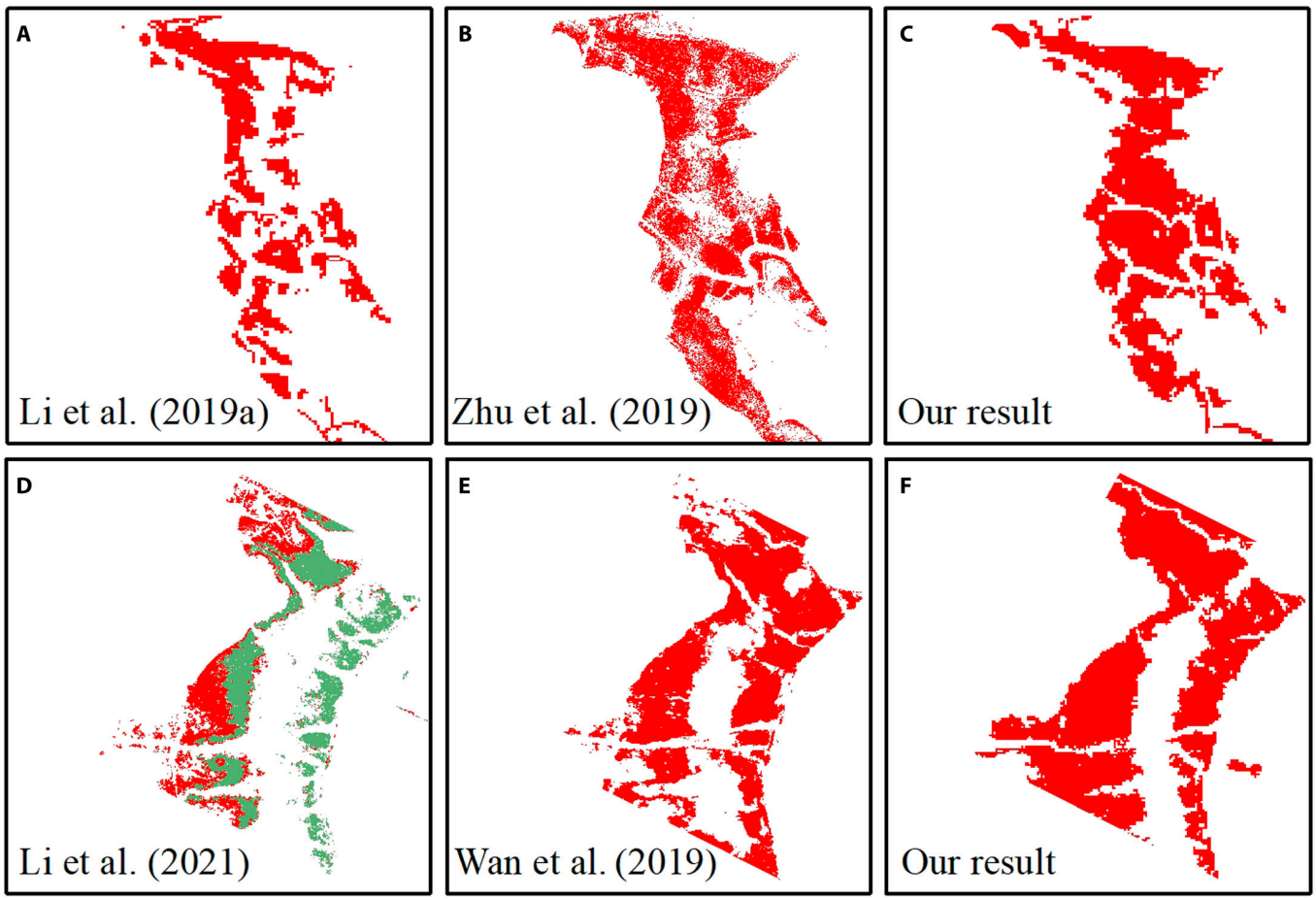

Fig. 5. Comparison of the generated national-scale map with accessible local maps in selected case areas (A to F). The red polygon represents *K. obovata*, while the green is the mixed *K. obovata* and *A. ilicifolius*.

of selected image pixels [19] and improve the separability among mangrove species with diverse payloads [35]. However, UAVs have limitations in addressing latitudinal gradients that exhibit large latitudinal spans. In larger areas, satellite-derived information for a given mangrove species, such as spectral bands and normalized difference vegetation index (NDVI) time series, is changing at different latitudes [20]. These variations lead to a loose decision surface that may include other land cover types in the target mangrove species during prediction.

The proposed approach attempted to utilize the change in separability caused by latitudinal gradients and explored the separability between *K. obovata* and its typically co-occurring mangrove species, *A. marina* and *A. corniculatum* (Table 4). For each pair of mangrove species, the northern case area had a larger separability than the southern case area in terms of J-M distance. The *K. obovata* and *A. marina* pairs were easier to distinguish than the other pairs in both case areas. The determined time period also contained image scenes with low separability, due to differences in mangrove species pairs and the requirement for a large time span to reduce the effects of clouds and shadows on the optical imagery.

Determining a time period with high separability from the target and its typically co-occurring mangrove species requires a denser time series of optical images, as the number of available images is severely affected by clouds. The chosen time period in this study overlapped with rainy days in the tropical and subtropical monsoon climates. Sentinel-1 synthetic aperture radar imagery is worth further exploration because of its tolerance to cloud cover.

Impacts of different feature selection methods

Three types of methods have been summarized in the field of feature selection: filter, wrapper, and embedded methods [55,56]. Filter methods evaluate features based on certain criteria, such as mutual information, and are thus independent of the classification algorithms. Wrapper methods rely on classification algorithms to judge the performance of potential feature combinations generated by diverse search strategies, such as genetic algorithms. Regarding the embedded methods, feature selection was integrated into the classification algorithm training phase, such as the feature importance metric of a trained RF.

One typical feature selection method was randomly selected from each type, that is, the mutual-information-based method, genetic-algorithm-based method, and RF-based method, to retrieve optimized features. We normalized the derived mutual information value, the occurring frequency of a feature, and feature importance to a range of 0 to 100, and plotted the top 15 features for comparison (Fig. 6). The rankings of the plotted features were quite different for each method. The first method supported that features derived from the time period having higher separability with adjacent mangrove species were more informative for classification. The second method emphasizes band ratios derived from near-infrared and short-wave infrared

Table 4. Separability between *K. obovata* and its typically co-occurred mangrove species of *A. marina* and *A. corniculatum*. Note: The northern and southern case areas are denoted by N and S, respectively. The image scenes within the determined time period are shown in italics, and the highest J-M distance values for each row are in bold.

		J-M distance											
K. obovata versus *A. marina*	N	Jan 14	Feb 18	Mar 22	*Apr 13*	*May 13*	*Jun 17*	*Jul 12*	*Aug 24*	*Sep 20*	Oct 18	Nov 22	Dec 22
		1.73	1.58	0.91	*1.83*	*1.39*	*1.96*	***1.98***	*1.91*	*1.80*	1.59	1.70	1.73
	S	Jan 15	Feb 19	Mar 15	Apr 9	*May 4*	*Jun 23*	*Jul 18*	*Aug 22*	*Sep 30*	Oct 26	Nov 25	Dec 30
		1.17	1.30	1.36	1.17	*0.85*	*0.77*	*1.51*	***1.83***	*1.49*	0.59	0.65	1.17
K. obovata versus *A. corniculatum*	N	Jan 14	Feb 18	Mar 22	*Apr 13*	*May 13*	*Jun 17*	*Jul 12*	*Aug 24*	*Sep 20*	Oct 18	Nov 22	Dec 22
		0.83	1.53	1.09	*1.74*	*0.81*	***1.83***	*1.60*	*1.22*	*1.48*	1.47	0.72	0.86
	S	Jan 15	Feb 19	Mar 15	Apr 9	*May 4*	*Jun 23*	*Jul 18*	*Aug 22*	*Sep 30*	Oct 26	Nov 25	Dec 30
		1.26	0.80	0.75	0.62	*1.08*	*1.20*	***1.36***	*0.87*	*1.31*	0.51	1.19	0.78

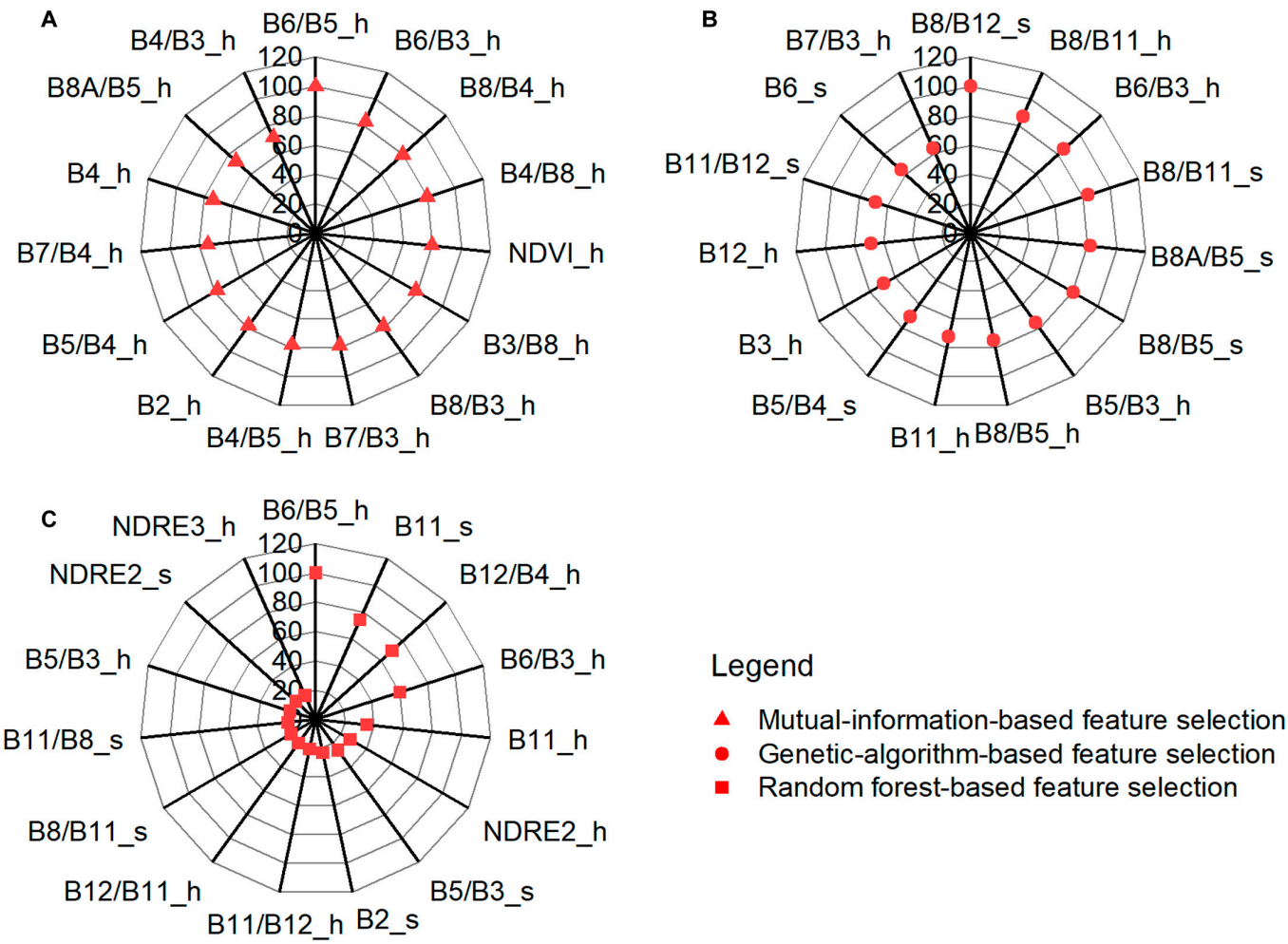

Fig. 6. The top 15 features using different feature selection methods (A to C). Features derived from the time period having higher separability with adjacent mangrove species are denoted with a suffix of _h, while those derived from the time period representing senescence season are denoted with a suffix of _s.

bands, while the third method emphasizes the features derived from the red-edge and short-wave infrared bands.

The top 15 features selected by the different feature selection methods were applied to retrieve the classification results using the RF algorithm (Fig. 7). The results were generally consistent for large patches; however, the details varied with different feature combinations. Therefore, we used the entire feature set to against the variations resulting from feature optimizations.

Limitations of the attempt to map national-scale *K. obovata*

As a first attempt to map *K. obovata* on a national scale, the resulting thematic map had some limitations. Compared with the results derived from high-spatial-resolution images [34–36] or those collected from UAV-based imagery [19], the results of this research may incorporate mixed samples with more than 1 mangrove species, leading to some exaggerated patches, especially at the edges (Fig. 8E and J). However, these results were not always consistent at the edges (Fig. 8B, G, and I), causing difficulties in accurate evaluation. This exaggeration may also result from a lack of adversarial samples representing other nearby mangrove species. Tuning the training samples based on this study is worth further exploration.

Although the mangrove map was used to define the extent of the study area, the thematic map was independent of the mangrove distribution map. For example, the identified mangrove area in Zhejiang province was 66.3 ha with a dominance of *K. obovata*, while the thematic map only captured 28.6 ha of it. This is because small patches were not well reflected by Sentinel-2 imagery, and later postprocessing only partly corrected the omission errors. Various factors can affect the appearance of a mangrove species, such as density, height, and health status, leading to hesitation in repairing omission errors. This problem would be alleviated if the distributions of *A. marina* and *A. corniculatum* were available, since these 3 mangrove species dominate the northern area.

Distribution patterns of *K. obovata* in China revealed by the generated map

On the basis of the generated map, the distribution patterns of *K. obovata* and its hot spots were analyzed using kernel density estimation (Fig. 9), which is a typical method for estimating the density of features within a bandwidth [57]. In addition to patch occurrence, area-weighted patch occurrence was analyzed to emphasize large *K. obovata* patches. The identified areas with a high distribution density were extracted, and *K. obovata* patches associated with those areas were mapped to show their actual distribution.

According to this analysis, 5 regions having a high density of patch occurrences with or without area weights were identified. Fujian province had the largest number of *K. obovata* patches (Fig. 9C), and its center was the Jiulong River Estuary for area-weighted patch occurrence (the identified patches in Luoyang River Estuary were fragmented; thus, the place became a center for patch occurrence). Shenzhen Bay has the largest area of *K. obovata*, including the Futian and Maipo Nature Reserves (Fig. 9D). The Tamsui River Estuary, characterized by a large population of *K. obovata* [58], was also identified using a thematic map (Fig. 9E). The Zhenhai Bay Reserve had more *K. obovata* patches (Fig. 9F), while its neighboring Yangjiang Port had larger areas of *K. obovata*, shifting the center for area-weighted patch occurrence.

Compared with the mangrove species occurrence dataset [59], the generated map can provide more updated, detailed,

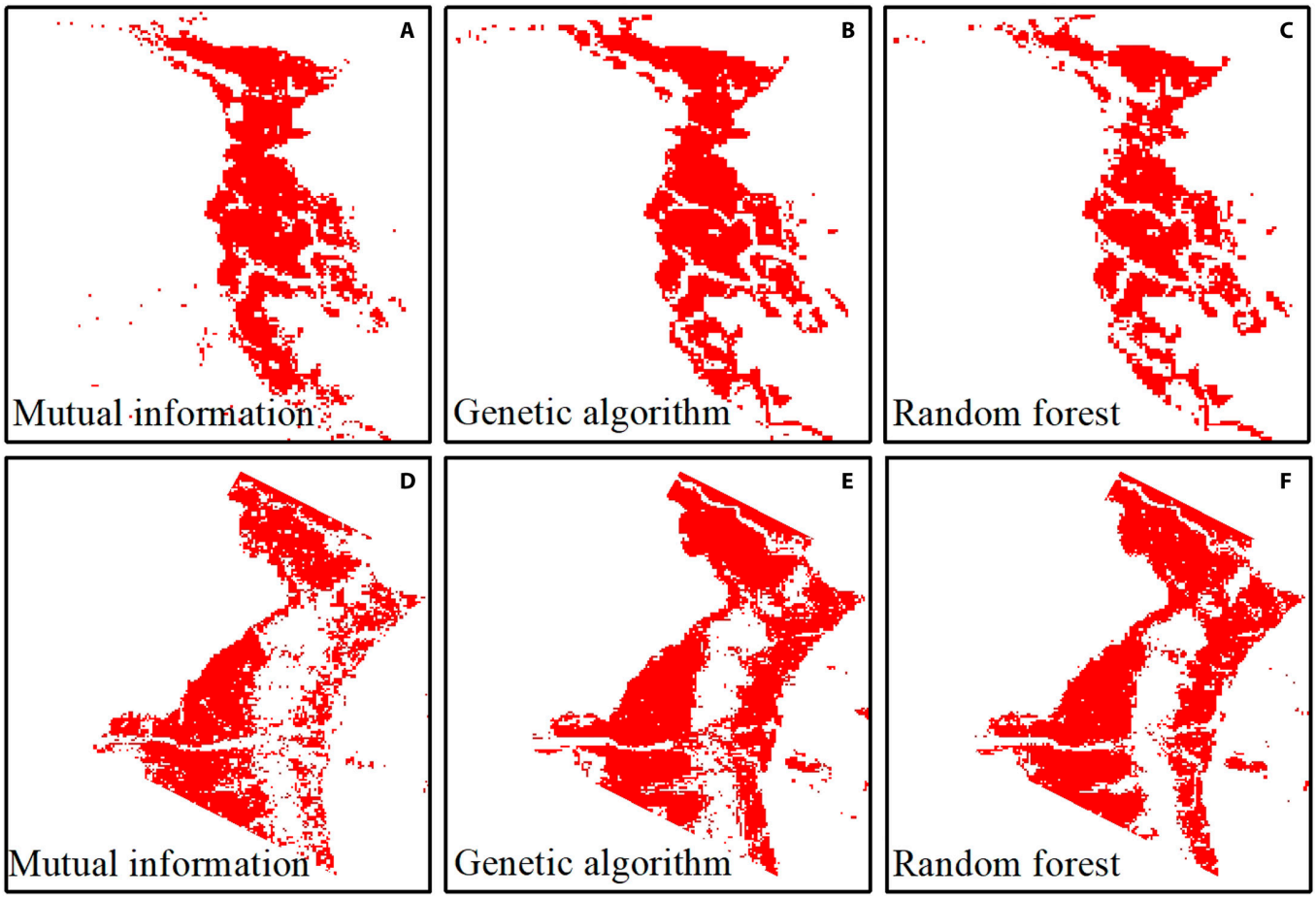

Fig. 7. Identified patches of *K. obovata* using the selected top 15 features by different feature selection methods (A to F).

and precise information on this mangrove species. The analysis not only retrieved the typical distribution of *K. obovata* but also benefited the assessment of suitable habitats for mangrove restoration.

Implications for sustainable mangrove management

Mangroves in China are under strict management of government. Since the 1990s, a series of laws and regulations have been formulated to protect mangroves and their habitats [60]. With the shift from the occupied area to its ecological restoration, there is an acute need for mangrove species distribution due to their varied characteristics in hydrological conditions, salinity tolerance, morphology, biomass, etc. After the Special Action Plan for Mangrove Protection and Restoration (2020–2025), the Technical Guide for Marine Ecological Restoration (Trial) was issued in 2021 [61], which emphasizes the use of native mangrove species including *K. obovata*. This study provides the first national-scale distribution of mangrove patches dominated by *K. obovata* and compensates field survey and experiment to determine the appropriate for planted seedlings and suitable planting sites along the coast.

Mangrove species are tightly linked to their health status, which serve as the foundation for sustainable mangrove management. Each mangrove species has specific diseases and pests, with damage often an exacerbated in large monographic patches [62]. For example, *Diaspididae* primarily infest the leaves of

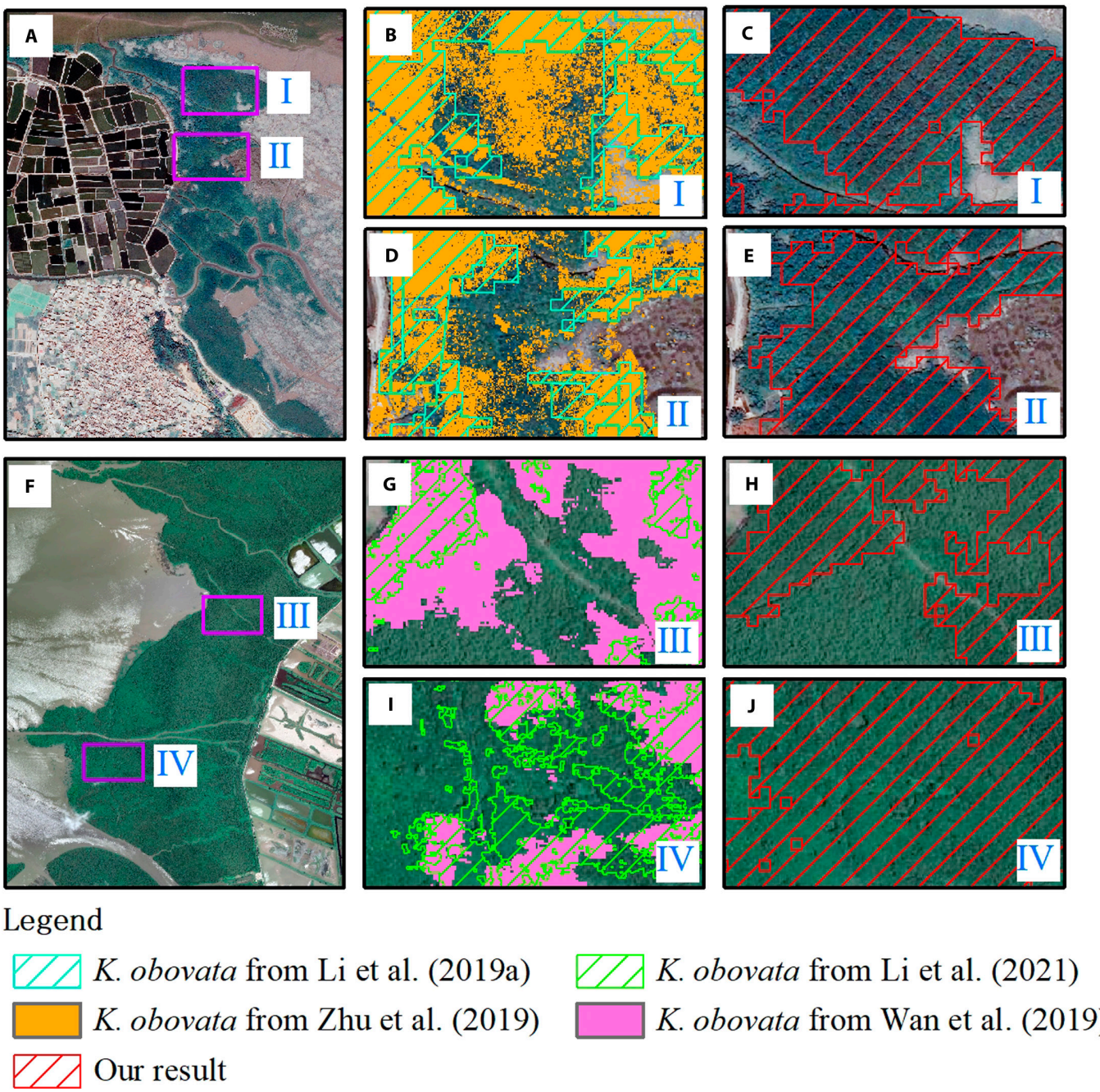

Fig. 8. Examples of inconsistent details for the 2 selected case areas (A to J). The mixed *K. obovata* and *A. ilicifolius* class in Li et al. [35] was merged into *K. obovata* in reference to Wan et al. [36].

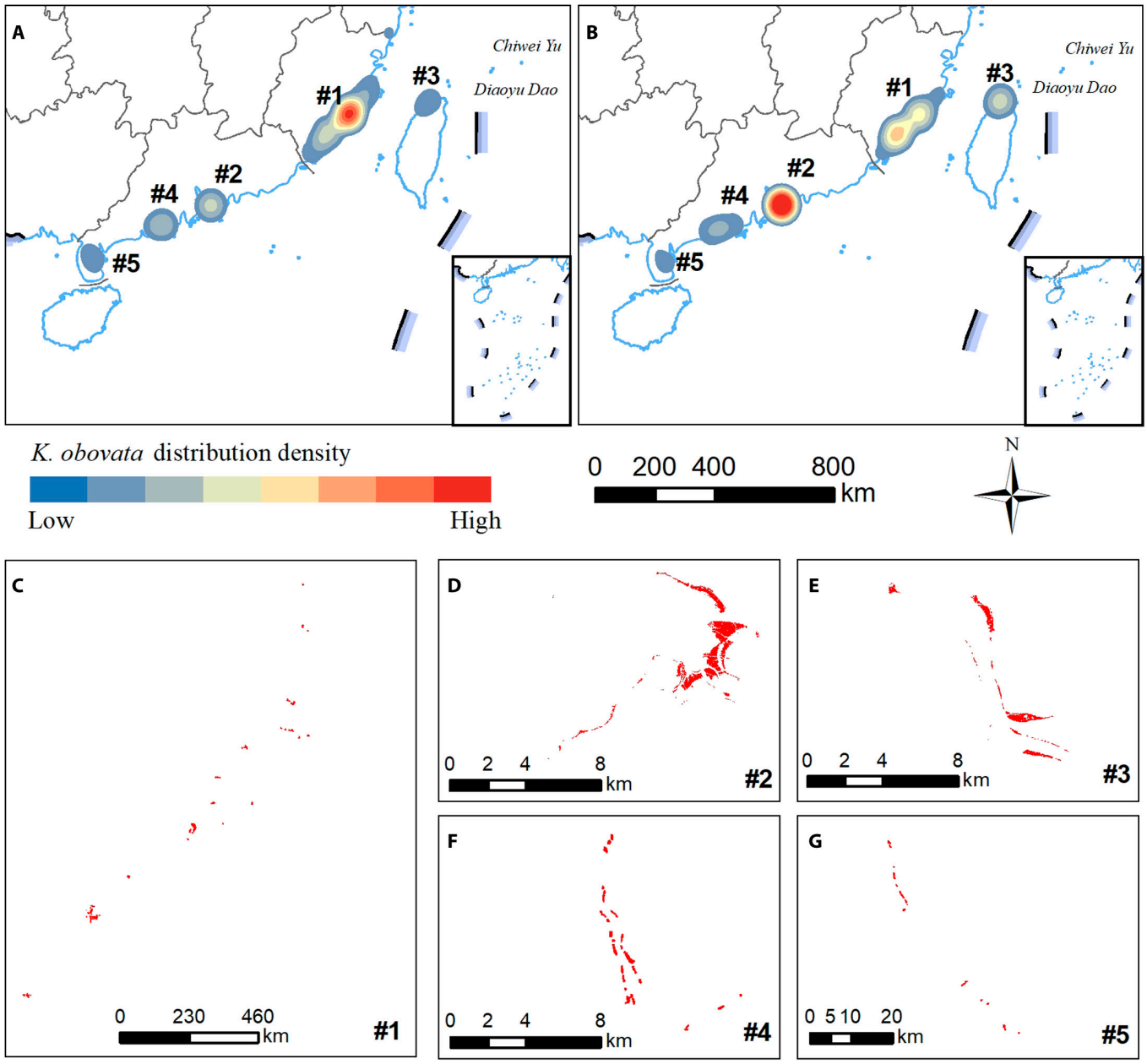

Fig. 9. Distribution patterns of *K. obovata* and its hot spots in China revealed by the generated map. The kernel density estimation is used to extract distribution patterns for (A) patch occurrence and (B) area-weighted patch occurrence, while the bandwidth is determined using a spatial variant of Silverman's rule of thumb. Dimensionless density values were represented using a color ramp (C to F). The plots used the map with an approval number of GS(2024)0610.

K. obovata during certain time periods. By integrating remote sensing and big data techniques, diseases and pests can be monitored, recorded, and predicted. Manual interventions, such as biological control, physical traps, and some chemical solutions, can prevent further degradation or mortality of certain mangrove species. Moreover, mangrove species have diverse morphology in roots, stems, and leaves, and stress monitoring should also be carried out for each species to account for species-specific effects [63]. The mangrove species distribution data is necessary for monitoring the health of specific mangrove species.

Engaging local communities is the key to sustainable mangrove management. Mangroves can provide resources such as honey and seafood, ecosystem services such as shoreline stabilization and carbon sequestration, as well as employment opportunities such as raising seedlings, planting, and patrolling mangroves. However, different mangrove species exhibit their characteristics. For instance, *A. corniculatum* is a good source of honey; *Rhizophora stylosa* has well-developed prop root to dissipate wave energy. Areas with concentrated distributions of a specific mangrove species can explore new ways to utilize them with high added value, such as ecological farming and ecotourism. Fragmented mangroves also contribute positively to local biodiversity, as ecosystem services respond nonlinearly to habitat size. Consequently, the *K. obovata* at its northern limit also holds significant values. The characteristics can be considered in natural resource accounting for mortgages. The transfer payments and the blue carbon trading market in China

can also bring additional revenue for local government [64]. Incorporating a detailed distribution of mangrove species can guarantee a reliable estimation of mangrove values. In 2021, a mangrove comanagement project was jointly launched by the Zhanjiang Mangrove National Nature Reserve Administration, the Society of Entrepreneurs and Ecology Foundation, and the Mangrove Foundation. This project attempts to incorporate local communities in decision-making and responsibility sharing. Similar to existing projects, social, economic, and ecological trade-offs worth further attentions for the implementation of sustainable mangrove management [65–67].

To solve the problem of limited generalizability of existing mangrove species mapping approaches along large latitudinal gradients, we took *K. obovata* in China as an example and proposed an approach to determine the separability time period based on J-M distance to distinguish it from its typically adjacent mangrove species. Separability was further enhanced using senescence images to eliminate the neighboring salt marshes. The resulting map achieved an OA value of 88.5%, and a qualitative comparison showed that the generated map was generally consistent with those derived from the local-scale results. The statistics showed that the total area of *K. obovata* in China for 2020 was 1,199 ha, and more than 92% of them were distributed in Fujian, Guangdong, Hong Kong, and Taiwan. Further analysis using kernel density estimation identified typical distribution areas of this mangrove species at the bay scale and found that Shenzhen Bay had the largest *K. obovata* area of 336.5 ha that mainly distributed in the Futian and Maipo Nature Reserves.

To the best of our knowledge, this study is the first attempt to map the nationwide distribution of *K. obovata*, which has the largest latitudinal span and tolerance to low temperatures in China. We also conducted the first national-scale analysis of spatial distribution patterns and hot spots when local-scale studies could not supply such information. The proposed approach has the potential to be applied to other mangrove species along latitudinal gradients, as local studies were sufficient to support the calculation of the separability metric J-M distance. The generated map is indispensable for species-specific applications in mangrove ecology and management.

In the future, the focus will be on optimizing the training samples to incorporate more adversarial samples that represent other nearby mangrove species. Such optimization may result in a more precise and consistent mangrove species map for studying its distribution, biomass, carbon storage, and other related ecosystem services.

Acknowledgments

Funding: This work was jointly supported by the National Key R&D Program of China (2022YFF1302000), the Open Research Program of the International Research Center of Big Data for Sustainable Development Goals (CBAS2022ORP06), the National Natural Science Foundation of China (42201422), the Youth Innovation Promotion Association of Chinese Academy of Sciences (2021227), and the National Earth System Science Data Center (www.geodata.cn). We also thank the Science and Technology Basic Resources Investigation Program of China (2017FY100700) for providing field sample plots with mangrove species composition.

Author contributions: C.Z. and M.J. designed the study. C.Z., R.Z., and X.G. conducted the data analysis. Z.W., D.M., and C.Z. provided guidance on data processing, methodology, and writing.

Competing interests: The authors declare that they have no competing interests.

Data Availability

Data are publicly available on a data repository Science Data Bank (https://doi.org/10.57760/sciencedb.13291).

References

1. Whitt AA, Coleman R, Lovelock CE, Gillies C, Ierodiaconou D, Liyanapathirana M, Macreadie PI. March of the mangroves: Drivers of encroachment into southern temperate saltmarsh. *Estuar Coast Shelf Sci*. 2020;240:Article 106776.
2. Sun W, Chen C, Liu W, Yang G, Meng X, Wang L, Ren K. Coastline extraction using remote sensing: A review. *GIScience Remote Sens*. 2023;60(1):Article 2243671.
3. Wu M, He Z, Fung S, Cao Y, Guan D, Peng Y, Lee SY. Species choice in mangrove reforestation may influence the quantity and quality of long-term carbon sequestration and storage. *Sci Total Environ*. 2020;714:Article 136742.
4. Chen J, Huang Y, Chen G, Ye Y. Effects of simulated sea level rise on stocks and sources of soil organic carbon in Kandelia obovata mangrove forests. *For Ecol Manage*. 2020;460:Article 117898.
5. Carnell PE, Palacios MM, Waryszak P, Trevathan-Tackett SM, Masqué P, Macreadie PI. Blue carbon drawdown by restored mangrove forests improves with age. *J Environ Manage*. 2022;306:Article 114301.
6. Giri C, Long J, Abbas S, Murali RM, Qamer FM, Pengra B, Thau D. Distribution and dynamics of mangrove forests of South Asia. *J Environ Manage*. 2015;148:101–111.
7. Wang L, Jia M, Yin D, Tian J. A review of remote sensing for mangrove forests: 1956–2018. *Remote Sens Environ*. 2019;231:Article 111223.
8. Long C, Dai Z, Zhou X, Mei X, Van CM. Mapping mangrove forests in the Red River Delta, Vietnam. *For Ecol Manage*. 2021;483:Article 118910.
9. Jia M, Wang Z, Mao D, Ren C, Song K, Zhao C, Wang C, Xiao X, Wang Y. Mapping global distribution of mangrove forests at 10-m resolution. *Sci. Bull.* 2023;68(12):1306–1316.
10. Dargan S, Kumar M, Ayyagari MR, Kumar G. A survey of deep learning and its applications: A new paradigm to machine learning. *Arch Compu. Methods Eng*. 2020;27:1071–1092.
11. Fu B, He X, Yao H, Liang Y, Deng T, He H, Fan D, Lan G, He W. Comparison of RFE-DL and stacking ensemble learning algorithms for classifying mangrove species on UAV multispectral images. *Int J Appl Earth Obs Geoinf*. 2022;112:Article 102890.
12. Zimudzi E, Sanders I, Rollings N, Omlin CW. Remote sensing of mangroves using unmanned aerial vehicles: Current state and future directions. *J Spat Sci*. 2021;66(2):195–212.
13. Immitzer M, Atzberger C, Koukal T. Tree species classification with random forest using very high spatial resolution 8-band WorldView-2 satellite data. *Remote Sens*. 2012;4(9):2661–2693.
14. Li Q, Wong FKK, Fung T. Classification of mangrove species using combined WordView-3 and LiDAR data in Mai Po nature reserve, Hong Kong. *Remote Sens*. 2019;11(18):2114.

15. Tamiminia H, Salehi B, Mahdianpari M, Quackenbush L, Adeli S, Brisco B. Google Earth Engine for geo-big data applications: A meta-analysis and systematic review. *ISPRS J. Photogramm Remote Sens*. 2020;164:152–170.
16. Huang K, Yang G, Yuan Y, Sun W, Meng X, Ge Y. Optical and SAR images Combined Mangrove Index based on multi-feature fusion. *Sci Remote Sens*. 2022;5:Article 100040.
17. Luo J, Ni G, Zhang Y, Wang K, Shen M, Cao Z, Qi T, Xiao Q, Qiu Y, Cai Y, et al. A new technique for quantifying algal bloom, floating/emergent and submerged vegetation in eutrophic shallow lakes using Landsat imagery. *Remote Sens Environ*. 2023;287:Article 113480.
18. Wang D, Wan B, Qiu P, Su Y, Guo Q, Wang R, Sun F, Wu X. Evaluating the performance of sentinel-2, landsat 8 and pléiades-1 in mapping mangrove extent and species. *Remote Sens*. 2018;10(9):1468.
19. Li H, Jia M, Zhang R, Ren Y, Wen X. Incorporating the plant phenological trajectory into mangrove species mapping with dense time series sentinel-2 imagery and the google earth engine platform. *Remote Sens*. 2019;11(21):2479.
20. Zhao C, Qin CZ, Wang Z, Mao D, Wang Y, Jia M. Decision surface optimization in mapping exotic mangrove species (Sonneratia apetala) across latitudinal coastal areas of China. *ISPRS J. Photogramm Remote Sens*. 2022;193:269–283.
21. Chen L, Wang W, Li QQ, Zhang Y, Yang S, Osland MJ, Huang J, Peng C. Mangrove species' responses to winter air temperature extremes in China. *Ecosphere*. 2017;8(6):Article e01865.
22. Pastor-Guzman J, Dash J, Atkinson PM. Remote sensing of mangrove forest phenology and its environmental drivers. *Remote Sens Environ*. 2018;205:71–84.
23. Xie Z, Zhao Y, Jiang R, Zhang M, Hammer G, Chapman S, Brider J, Potgieter AB. Seasonal dynamics of fallow and cropping lands in the broadacre cropping region of Australia. *Remote Sens Environ*. 2024;305:Article 114070.
24. Su W, Ye C, Zhang Y, Hao S, Li QQ. Identification of putative key genes for coastal environments and cold adaptation in mangrove Kandelia obovata through transcriptome analysis. *Sci Total Environ*. 2019;681:191–201.
25. Zhao C, Jia M, Wang Z, Mao D, Wang Y. Toward a better understanding of coastal salt marsh mapping: A case from China using dual-temporal images. *Remote Sens Environ*. 2023;295:Article 113664.
26. Sun C, Li J, Liu Y, Liu Y, Liu R. Plant species classification in salt marshes using phenological parameters derived from Sentinel-2 pixel-differential time-series. *Remote Sens Environ*. 2021;256:Article 112320.
27. Fan H, Wang W. Some thematic issues for mangrove conservation in China. *J Xiamen Univ Nat Sci*. 2017;56:323–330.
28. Pan L-h, Shi X, Zeng C, Chen Y. The plant types of mangroves in Guangxi. *Guangxi Sci*. 2018;25:352–362.
29. Davis CC, Lyra GM, Park DS, Asprino R, Maruyama R, Torquato D, Cook BI, Ellison AM. New directions in tropical phenology. *Trends Ecol Evol*. 2022;37(8):683–693.
30. He Z, Xu S, Zhang Z, Guo W, Lyu H, Zhong C, Boufford DE, Duke NC, The International Mangrove Consortium, Shi S. Convergent adaptation of the genomes of woody plants at the land–sea interface. *Natl Sci Rev*. 2020;7:978–993.
31. Gunal S, Edizkan R. Subspace based feature selection for pattern recognition. *Inf Sci*. 2008;178(19):3716–3726.
32. Ferreira MP, Grondona AEB, Rolim SBA, Shimabukuro YE. Analyzing the spectral variability of tropical tree species using hyperspectral feature selection and leaf optical modeling. *J Appl Remote Sens*. 2013;7:Article 073502.
33. Sen R, Goswami S, Mandal AK, Chakraborty B. An effective feature subset selection approach based on Jeffries-Matusita distance for multiclass problems. *J Intell Fuzzy Syst*. 2022;42:4173–4190.
34. Zhu X, Hou Y, Weng Q, Chen L. Integrating UAV optical imagery and LiDAR data for assessing the spatial relationship between mangrove and inundation across a subtropical estuarine wetland. *ISPRS J Photogramm Remote Sens*. 2019;149:146–156.
35. Li Q, Wong FKK, Fung T. Mapping multi-layered mangroves from multispectral, hyperspectral, and LiDAR data. *Remote Sens Environ*. 2021;258:Article 112403.
36. Wan L, Zhang H, Lin G, Lin H. A small-patched convolutional neural network for mangrove mapping at species level using high-resolution remote-sensing image. *Ann GIS*. 2019;25:45–55.
37. Tian J, Wang L, Yin D, Li X, Diao C, Gong H, Shi C, Menenti M, Ge Y, Nie S, et al. Development of spectral-phenological features for deep learning to understand Spartina alterniflora invasion. *Remote Sens Environ*. 2020;242:Article 111745.
38. Chen G, Jin R, Ye Z, Li Q, Gu J, Luo M, Luo Y, Christakos G, Morris J, He J, et al. Spatiotemporal mapping of salt marshes in the intertidal zone of China during 1985–2019. *J Remote Sens*. 2022;2022:Article 9793626.
39. Behera MD, Barnwal S, Paramanik S, Das P, Bhattyacharya BK, Jagadish B, Roy PS, Ghosh SM, Behera SK. Species-level classification and mapping of a mangrove forest using random forest—utilisation of AVIRIS-NG and sentinel data. *Remote Sens*. 2021;13(11):2027.
40. Pham TD, Yokoya N, Bui DT, Yoshino K, Friess DA. Remote sensing approaches for monitoring mangrove species, structure, and biomass: Opportunities and challenges. *Remote Sens*. 2019;11(3):230.
41. Sukawattanavijit C, Chen J, Zhang H. GA-SVM algorithm for improving land-cover classification using SAR and optical remote sensing data. *IEEE Geosci Remote Sens Lett*. 2017;14(3):284–288.
42. Fox EW, Hill RA, Leibowitz SG, Olsen AR, Thornbrugh DJ, Weber MH. Assessing the accuracy and stability of variable selection methods for random forest modeling in ecology. *Environ Monit Assess*. 2017;189(7):316.
43. Zhao C, Qin C-Z. Identifying large-area mangrove distribution based on remote sensing: A binary classification approach considering subclasses of non-mangroves. *Int J Appl Earth Obs Geoinf*. 2022;108:Article 102750.
44. Zhao C, Qin C-Z. The key reason of false positive misclassification for accurate large-area mangrove classifications. *Remote Sens*. 2021;13(15):2909.
45. Qiu P, Wang D, Zou X, Yang X, Xie G, Xu S, Zhong Z. Finer resolution estimation and mapping of mangrove biomass using UAV LiDAR and worldview-2 data. *Forests*. 2019;10:871.
46. Fu B, Liang Y, Lao Z, Sun X, Li S, He H, Sun W, Fan D. Quantifying scattering characteristics of mangrove species from Optuna-based optimal machine learning classification using multi-scale feature selection and SAR image time series. *Int J Appl Earth Obs Geoinf*. 2023;122:Article 103446.
47. Peng L, Liu K, Cao J, Zhu Y, Li F, Liu L. Combining GF-2 and RapidEye satellite data for mapping mangrove species using ensemble machine-learning methods. *Int J Remote Sens*. 2020;41(3):813–838.

48. Ma Y, Wu P, Pan L, Wang J, Wang J, Ren G, Ma Y. Classification and coverage estimation of mangrove species at the Maoweihai Sea in Guangxi based on GF-2 images. *Mar Sci*. 2019;43:60–70.
49. Zheng Y et al. Mangrove inter-species classification based on ZY-3 images in Leizhou Peninsula, Guangdong Province. *Remote Sens Land Resour*. 2019;31:201–208.
50. Xin K, Yan K, Gao C, Li Z. Carbon storage and its influencing factors in Hainan Dongzhangang mangrove wetlands. *Mar Freshw Res*. 2018;69:771–779.
51. Belgiu M, Drăguț L. Random forest in remote sensing: A review of applications and future directions. *ISPRS J Photogramm Remote Sens*. 2016;114:24–31.
52. Yang G, Huang K, Sun W, Meng X, Mao D, Ge Y. Enhanced mangrove vegetation index based on hyperspectral images for mapping mangrove. *ISPRS J Photogramm Remote Sens*. 2022;189:236–254.
53. Zhao C-P, Qin C-Z. A detailed mangrove map of China for 2019 derived from Sentinel-1 and -2 images and Google Earth images. *Geosci Data J*. 2021;9(1):74–88.
54. Chakraborty T, Bhuniya D, Chatterjee M, Rahaman M, Singha D, Chatterjee BN, Datta S, Rana A, Samanta K, Srivastawa S, et al. Acanthus ilicifolius plant extract prevents DNA alterations in a transplantable Ehrlich ascites carcinoma-bearing murine model. *World J Gastroenterol*. 2007;13(48):6538–6548.
55. Chandrashekar G, Sahin F. A survey on feature selection methods. *Comput Electr Eng*. 2014;40:16–28.
56. Huang Y, Zhao C, Yang H, Song X, Chen J, Li Z. Feature selection solution with high dimensionality and low-sample size for land cover classification in object-based image analysis. *Remote Sens*. 2017;9(9):939.
57. Cai X, Wu Z, Cheng J. Using kernel density estimation to assess the spatial pattern of road density and its impact on landscape fragmentation. *Int J Geogr Inf Sci*. 2013;27:222–230.
58. Shih S-S. Spatial habitat suitability models of mangroves with Kandelia obovata. *Forests*. 2020;11(4):477.
59. Sahana M, Areendran G, Sajjad H. Assessment of suitable habitat of mangrove species for prioritizing restoration in coastal ecosystem of Sundarban Biosphere Reserve India. *Sci Rep*. 2022;12(1):20997.
60. Jia M, Wang Z, Zhang Y, Mao D, Wang C. Monitoring loss and recovery of mangrove forests during 42 years: The achievements of mangrove conservation in China. *Int J Appl Earth Obs Geoinf*. 2018;73:535–545.
61. Wang J, Liu Y, Liu M, Wang S, Zhang J, Wu H. Multi-phase environmental impact assessment of marine ecological restoration project based on DPSIR-cloud model. *Int J Environ Res Public Health*. 2022;19(20):13295.
62. Yang S, Peng J, Xue Y, Zheng Z, Zhou H. Species and integrated control of pests in mangrove community in China. *For Pest Dis*. 2020;1:32–41.
63. Reinert F, de Pinho CF, Ferreira MA. Diagnosing the level of stress on a mangrove species (Laguncularia racemosa) contaminated with oil: A necessary step for monitoring mangrove ecosystems. *Mar Pollut Bull*. 2016;113(1–2):94–99.
64. Li X, Wang D. Does transfer payments promote low-carbon development of resource-exhausted cities in China? *Earths Future*. 2022;10(1):e2021EF002339.
65. Huang L, Li X, Fang H, Yin D, Si Y, Wei J, Liu J, Hu X, Zhang L. Balancing social, economic and ecological benefits of reservoir operation during the flood season: A case study of the Three Gorges Project China. *J Hydrol*. 2019;572:422–434.
66. Datta D, Chattopadhyay R, Guha P. Community based mangrove management: A review on status and sustainability. *J Environ Manage*. 2012;107:84–95.
67. Mahmood H, Ahmed M, Islam T, Uddin MZ, Ahmed ZU, Saha C. Paradigm shift in the management of the Sundarbans mangrove forest of Bangladesh: Issues and challenges. *Trees For. People*. 2021;5:Article 100094.